26 days of age, when the most advanced differentiated cells are round spermatids (Fig. 3B). This early reduction cannot be explained by the lack of elongated spermatids in *Trf2*$^{-/-}$ testes, because in normal *Trf2*$^{+/+}$ testes these cells do not appear until 28 days of age (Fig. 1C). In contrast, the *Mcs* and *Gapd-s* genes were expressed at comparable levels in *Trf2*$^{-/-}$ and wild-type testes at 26 days of age (Fig. 3B), indicating gene-selective effects of TRF2 at this stage. Although the *Mcs* and *Gapd-s* genes did show reduced expression after 28 days of age, this likely reflects the absence of elongated spermatids at these later stages, and the overall reduction was still far less severe than that observed for the *Tp 1*, *Protamine 1*, and *Hsc70t* genes. These data from the juvenile testis analyses suggest that even though many genes are actively transcribed during the early phase of spermatid differentiation (*24*), TRF2 may not have a general role in the augmentation of overall levels of polymerase II transcription. Instead, it might regulate the differentiation program for spermiogenesis through its ability to selectively activate specific downstream target genes in round spermatids.

We noted that mice lacking the transcriptional activator CREM (cyclic AMP–responsive element modulator) also show a disruption in spermiogenesis (*13, 25*). However, our *Trf2*$^{-/-}$ mice exhibit a developmental block at a later step of spermatid differentiation, as judged from histological and marker gene expression analyses. In addition, an analysis during juvenile testis development revealed no significant differences between *Trf2*$^{-/-}$ and *Trf2*$^{+/+}$ testes in the expression of CREM (*26*) and the testis-specific CREM coactivator FHL4 (*27*), especially when normalized to *Gapdh* expression (Fig. 3C). Moreover, TRF2 deficiency had only a moderate effect on expression of the CREM coactivator ACT (*28*) (Fig. 3C).

Through targeted inactivation, we demonstrated the importance of TRF2 in the normal differentiation program of mouse spermiogenesis. The specific effects of the *Trf2* mutation on spermiogenesis indicate that *Trf2*$^{-/-}$ mice could be valuable for the study of some types of idiopathic infertility in men (*29*). Our study reveals that the physiological consequences of *Trf2* deficiency in mouse differ from those of TRF2 deficiencies in *C. elegans* and *Xenopus* (*8–10*). The normal embryonic development of *Trf2*$^{-/-}$ mice is most likely not a result of a maternal contribution of normal TRF2 protein, because *Trf2*$^{-/-}$ females are fertile. On the other hand, the embryonic lethal phenotypes in *C. elegans* and *Xenopus* have prevented further analyses of the possibility that TRF2 has an additional role(s) in male germ cell differentiation in these organisms. The functions of TRF2 might reflect differences in TRF2 expression patterns in these organisms (*5, 8–10*) or differences in TRF2 protein sequences, even though these proteins appear homologous among different species (*2*). Particularly, we note that mouse TRF2 is composed mainly of a core region of 180 amino acids, with a very short NH_2-terminal region, whereas the *C. elegans* TRF2 has a much longer NH_2-terminal sequence, an additional COOH-terminal sequence, and an insertion of ~100 amino acids in the core region (*2*). Another possibility is that the biological functions mediated by TBP and TRF2 may be distinct in different species. We propose that TBP or another protein may have taken over the role of TRF2 in mouse embryonic development and that TRF2 functions may have become restricted to specialized functions in the testis.

References and Notes

1. S. K. Burley, R. G. Roeder, *Annu. Rev. Biochem.* **65**, 769 (1996).
2. J. C. Dantonel, J. M. Wurtz, O. Poch, D. Moras, L. Tora, *Trends Biochem. Sci.* **24**, 335 (1999).
3. S. K. Hansen, S. Takada, R. H. Jacobson, J. T. Lis, R. Tjian, *Cell* **91**, 71 (1997).
4. T. Ohbayashi, Y. Makino, T. Tamura, *Nucleic Acids Res.* **27**, 750 (1999).
5. M. Teichmann *et al.*, *Proc. Natl. Acad. Sci. U.S.A.* **96**, 13720 (1999).
6. S. Takada, J. T. Lis, S. Zhou, R. Tjian, *Cell* **101**, 459 (2000).
7. M. C. Holmes, R. Tjian, *Science* **288**, 867 (2000).
8. L. Kaltenbach, M. A. Horner, J. H. Rothman, S. E. Mango, *Mol. Cell* **6**, 705 (2000).
9. J. C. Dantonel, S. Quintin, L. Lakatos, M. Labouesse, L. Tora, *Mol. Cell* **6**, 715 (2000).
10. G. J. C. Veenstra, D. L. Weeks, A. P. Wolffe, *Science* **290**, 2312 (2000).
11. Supplementary information is available on *Science* Online (www.sciencemag.org/cgi/content/full/1059188/DC1).
12. A. R. Bellve *et al.*, *J. Cell Biol.* **74**, 68 (1977).
13. F. Nantel *et al.*, *Nature* **380**, 159 (1996).
14. D. Zhang, in preparation.
15. S. Kashiwabara, Y. Arai, K. Kodaira, T. Baba, *Biochem. Biophys. Res. Commun.* **173**, 240 (1990).
16. Z. F. Zakeri, D. J. Wolgemuth, C. R. Hunt, *Mol. Cell. Biol.* **8**, 2925 (1988).
17. B. Drabent, C. Bode, B. Bramlage, D. Doenecke, *Histochem. Cell Biol.* **106**, 247 (1996).
18. M. Matsumoto, H. Fujimoto, *Biochem. Biophys. Res. Commun.* **166**, 43 (1990).
19. K. C. Kleene *et al.*, *Dev. Biol.* **137**, 395 (1990).
20. J. E. Welch, E. C. Schatte, D. A. O'Brien, E. M. Eddy, *Biol. Reprod.* **46**, 869 (1992).
21. K. D. Fulcher *et al.*, *Biol. Reprod.* **52**, 41 (1995).
22. D. Wouters-Tyrou, A. Martinage, P. Chevaillier, P. Sautiere, *Biochimie* **80**, 117 (1998).
23. Y. E. Yu *et al.*, *Proc. Natl. Acad. Sci. U.S.A.* **97**, 4683 (2000).
24. E. M. Eddy, *Semin. Cell Dev. Biol.* **9**, 451 (1998).
25. J. A. Blendy, K. H. Kaestner, G. F. Weinbauer, E. Nieschlag, G. Schutz, *Nature* **380**, 162 (1996).
26. R. Behr, N. Hunt, R. Ivell, J. Wessels, G. F. Weinbauer, *Biol. Reprod.* **62**, 1344 (2000).
27. G. M. Fimia, D. De Cesare, P. Sassone-Corsi, *Mol. Cell. Biol.* **20**, 8613 (2000).
28. ———, *Nature* **398**, 165 (1999).
29. T. Diemer, C. Desjardins, *Hum. Reprod. Update* **5**, 120 (1999).

30. We are grateful to the Laboratory of Animal Research Center of the Rockefeller University for mouse work. We also thank M. Hardy, M. Ito, and U. Kim for technical help and for critical discussion of the manuscript. This work was supported by NIH grants to R.G.R and P.L.M and by postdoctoral fellowships from the Norman Winston Foundation to D.Z. and from Deutsche Forschungsgemeinschaft Leukemia Research Foundation to M.T.

19 January 2001; accepted 3 April 2001
Published online 12 April 2001;
10.1126/science.1059188
Include this information when citing this paper.

The Foot-and-Mouth Epidemic in Great Britain: Pattern of Spread and Impact of Interventions

Neil M. Ferguson,* Christl A. Donnelly, Roy M. Anderson

We present an analysis of the current foot-and-mouth disease epidemic in Great Britain over the first 2 months of the spread of the virus. The net transmission potential of the pathogen and the increasing impact of control measures are estimated over the course of the epidemic to date. These results are used to parameterize a mathematical model of disease transmission that captures the differing spatial contact patterns between farms before and after the imposition of movement restrictions. The model is used to make predictions of future incidence and to simulate the impact of additional control strategies. Hastening the slaughter of animals with suspected infection is predicted to slow the epidemic, but more drastic action, such as "ring" culling or vaccination around infection foci, is necessary for more rapid control. Culling is predicted to be more effective than vaccination.

A new epidemic of foot-and-mouth disease (FMD) (also known as hoof-and-mouth disease) began in Great Britain in February 2001, 34 years since the last major outbreak. From the primary infection of a pig herd in Northumberland in early February, the disease spread rapidly via long-distance animal movements and also spread locally via contact and windborne transmission (*1*). The initial spread was greatly influenced by the fre-

quency of movement of animals around the country and by their mixing in livestock markets. Particular infection foci are Cumbria, Dumfries, and Galloway (CDG) and Devon (Fig. 1). Subsequently, local transmission largely determined the pattern of spread.

The disease is caused by a highly contagious aphthovirus in the family Picornaviridae, which persists as distinct antigenic types, each consisting of multiple strains in various regions of the world (though Europe had been largely free of infection for many years). The antigenic type responsible for the current epidemic is FMD type O, Pan Asia strain. The virus can persist outside the host for a month or more in damp soil, aided by cold temperatures. Plumes of virus contained within droplets, excreted at very high concentrations from symptomatic animals, are dispersed by wind over long distances (up to 60 km over land and 250 km over water) (*2*, *3*).

The virus infects many cloven-footed mammals, including cattle, sheep, goats, deer, and pigs. The typical severity of the disease and the level and duration of infectiousness vary widely, with sheep showing less clinical evidence of infection (particularly with the O Pan Asia strain of the virus) than cattle or pigs. Most animals recover from infection, albeit with permanently reduced weight gain or milk yield, though mortality can be high in the young. Current control policies in Europe are based on strict import and quarantine regulations, after a period of routine vaccination that ended in 1991 (*4*). Immunization by high-potency vaccines (inactivated, concentrated, purified preparations of virus mixed with an adjuvant) takes 3 to 4 days in cattle and sheep to induce protective immunity but may only protect for a limited period (4 to 6 months for one dose of emergency high-potency vaccine), in part because of antigenic evolution and diversity in the virus. Vaccinated animals exposed to infection may develop subclinical infection and secrete virus (*5*–*8*).

The epidemic started roughly 2 weeks before the initial report of infection in pigs on 19 February 2001 (*1*). Subsequently, the first species infected on the affected farms was almost always sheep (53%) or cattle (45%) rather than pigs (1%). In addition to the policy of slaughtering animals on infected farms, on 23 February further control measures were initiated, including a ban on all animal movements, the closure of markets, and restricted public use of footpaths across agricultural land (*1*). Contact tracing for all FMD-affected farms has produced unique data on the spatial scale of disease transmission (provided by the British Ministry of Agriculture, Fisheries and Food), clearly demonstrating that farms closest to index cases of FMD are at greatest risk of infection (Fig. 2A). Analysis of data on infectious contacts between farms indicated that movement restrictions resulted in a drop in the proportion of transmission events occurring over a distance of 9 km or more from 38 to 12% (*9*). The transmission potential of an infectious agent is quantified by the basic reproductive number, R_0, which measures the average number of secondarily infected farms generated by one primary infection in an entirely susceptible group of farms (*10*). To stop further spread and prevent a large epidemic, the value of R_0 must be reduced to less than unity. Using the contact tracing data, we directly estimated (*11*) that movement restrictions resulted in a drop in the minimum bounds on R_0 from 4.5 to 1.6.

Data on the distribution of distances to all Great Britain farms from FMD-affected farms, weighted by the relative contact probability of farms as a function of distance (*12*) (Fig. 2A), yielded an estimated effective neighborhood size of 6.7 in units of nearest neighbor farms. We estimate that farms 0.5, 1, and 1.5 km away from a single farm affected by FMD would have probabilities 0.26, 0.06, and 0.02, respectively, of becoming infected.

The temporal evolution of the epidemic and its future course depend in part on the distributions of the times between the four key events recorded in current surveillance and control efforts: (i) infection of a farm (determined retrospectively through the examination of lesions), (ii) the report of a suspect infection, (iii) confirmation of disease, and (iv) slaughter of the animals on the infected farm. Previous research has identified the importance of these delays in determining the impact of slaughter policies on the pattern of the epidemic (*13*). The infection-to-report distribution was estimated from the observed data corrected for right censoring (Fig. 2B) (only confirmed cases are included in our data set, and very recent reports of infection may not yet have been confirmed). These data indicate that the infection-to-report distribution varies by species first infected (Fig. 2B) and that both distributions have changed over time (Fig. 2C). The infection-to-report distributions are amalgams of the underlying biological distributions of the time from infection to development of clinical signs of disease [on which experimental infection data are limited (*14*)] and the influence of other factors (including variability in case definition and in surveillance efficiency). The reductions in the average delays represented by these distributions through time have important consequences for the predicted magnitude of the epidemic through their impact in reducing R_0.

A mathematical epidemic model (*15*) was fitted to the three fully recorded incidence time series (report, confirmation, and slaughter), with the farm used as the basic unit of study. The model combined a traditional mass-action transmission term, to describe initial long-range contacts, with a spatial correlation structure (*16*), to capture the locality of later transmission and the structure of the contact network between neighboring farms.

Department of Infectious Disease Epidemiology, Imperial College School of Medicine, St. Mary's Campus, Norfolk Place, London W2 1PG, UK.

*To whom correspondence should be addressed. E-mail: Neil.Ferguson@ic.ac.uk

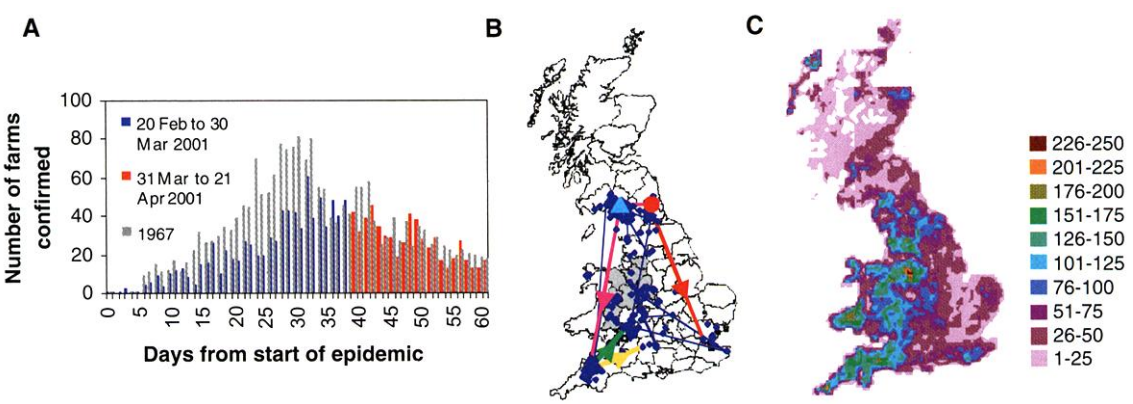

Fig. 1. Comparison of the temporal and spatial patterns of the 1967–68 and 2001 FMD epidemics. (**A**) Time series of confirmed cases (*1*, *18*). (**B**) Map of 2001 FMD cases recorded by 30 March 2001 (*1*). The original infection is mapped with a red circle, and Longtown Market is mapped with a light blue triangle. Traced contacts between farms are shown with connecting lines, with transmission contacts to Essex (red), Devon (purple), Wiltshire (gold), and Hereford (green) highlighted. The counties most affected in 1967–68 are highlighted in gray. (**C**) Map of number of holdings with sheep, cattle, and/or pigs in 10-km squares, using data from the June 2000 Agricultural and Horticultural Census (*19*).

By tracking the disease state of connected farms within the contact network, the model structure lends itself to the evaluation of control strategies based on local control around sites of infection. A deterministic compartmental model was used to permit robust parameter estimation and allow the estimated time-varying delay distributions (Fig. 2) to be realistically reproduced. Spatially explicit stochastic models will therefore complement this framework in future, and it will be interesting to compare the utility of the two approaches. For numerical tractability, we did not differentiate between host species but instead used a time-varying infection-to-report distribution averaged over species. The population of farms was stratified into five classes: susceptible, asymptomatically infected but not infectious, infectious but not reported, infectious and reported, and slaughtered (assumed uninfectious). We assume that all infected farms will eventually be identified by surveillance. From the contact data, we estimated the connectedness of the contact network, ϕ, and the effective neighborhood size, n. Three key parameters (the date of the first infection and R_0 before and after the introduction of movement restrictions) were estimated by fitting the model to the recorded incidence time series (assuming the data were Poisson distributed). The sensitivity of model results to the value of one other key parameter, not reliably estimable with current data (the infectiousness of a farm after the disease has been reported relative to that just before reporting, r_I), was explored.

The quality of fit of the model to the data was good (Fig. 3, A through C), given the fluctuating nature of daily case reports. Incidence predictions are plotted (Fig. 3D) for the best fit model and for the parameter sets corresponding to the upper and lower 95% confidence bounds on predicted total epidemic size (measured by R_0). The 95% confidence bounds on the final size of the epidemic were estimated as 44 to 64% of the population at risk. Here we assume the population at risk to be the approximately 45,000 farms in the currently infected areas in Great Britain, under the presumption that infection is prevented from spreading further. However, if such control fails, the susceptible population would approach the entire national total of 131,000 farms and the total epidemic sizes would be proportionately larger. The model-estimated 95% confidence interval for R_0 immediately after movement restrictions were imposed was 1.5 to 1.8 (falling to 1.2 to 1.4 by 28 March), when $r_I = 1$, which is in excellent agreement with the estimate obtained directly from the contact data. Slightly higher R_0 values were obtained if lower r_I values were assumed, due to the shorter generation time between rounds of infection, and lower R_0 estimates obtained for larger values of r_I.

We explored the sensitivity of model predictions to regional heterogeneity in transmission intensity by estimating key delay distributions and fitting the model separately for the CDG infected area and for all other infected areas combined (Fig. 3E). Best estimates of R_0 on 28 March are 1.7 for CDG and 1.1 in other areas, indicating that transmission is significantly more intense (and the epidemic more established) in the former area. In obtaining the non-CDG estimate, we combined data from multiple spatially disconnected regions, each with small numbers of cases (which largely precludes their individual analysis), thereby averaging over probable additional regional heterogeneity in R_0 (in some regions, R_0 may be below 1 already but remain substantially above 1 in others).

The options for the control of a highly contagious disease, in an environment where the major host species are densely aggregated and frequently moved, depend on effective surveillance and rapid destruction of animals on farms on which cases of infection arise. Because of logistical difficulties in processing very large numbers of animals (1,896,000 had already been slaughtered by 22 April, compared to 440,000 during the whole of the 1967–68 epidemic), there were initially substantial delays (Fig. 2) between the reporting of a suspect case and culling of the farm. These only began to be overcome late in March (Fig. 2C). Our analysis shows (Fig. 4A) that achieving the goal of slaughtering on all farms within 24 hours of case reporting without necessarily waiting for laboratory confirmation (which became UK government policy in late March) can significantly slow the epidemic. However, such improvements in slaughter times fail to reduce R_0 below 1 under the assumption that the infectivity of farms after disease reporting is at the same level as that before ($r_I = 1$), and only results in rapid control if we assume that infectivity increases throughout the time from infection to slaughter and hence peaks after the disease is diagnosed on a farm (the $r_I = 5$ curve in Fig. 4A). In the latter scenario, a small reduction in slaughter times results in a disproportionate reduction in R_0, making it more likely that more rapid slaughter alone will achieve $R_0 < 1$. However, because data do not exist with which to estimate the infectiousness of a farm as a function of time since infection, prudence dictates that in addition to more rapid culling of infected farms, it is necessary

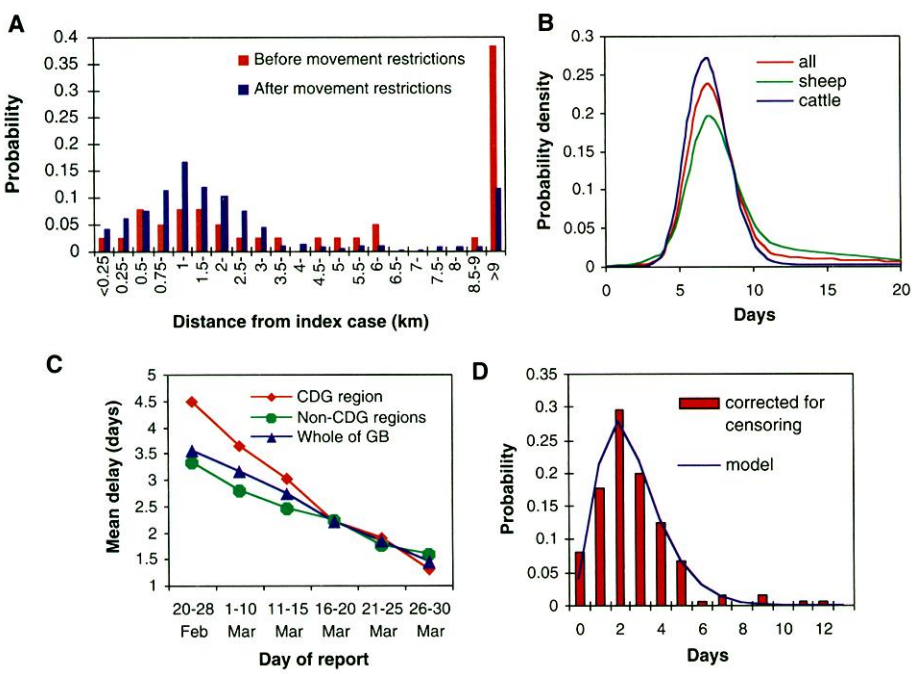

Fig. 2. (**A**) The observed distribution of distances between infectious contacts. Before and after the introduction of movement restrictions, 38 and 12% of distances, respectively, are greater than 9 km. The proportion of contacts beyond 9 km is a combination of the mass action probability (21 and 4%, before and after the introduction of movement restrictions, respectively) and the probability of local spread beyond 9 km (9). (**B**) Estimated distributions of the infection-to-report delay, allowing for censoring, for all cases and stratified by the species first infected (with means of 9.5 and 8.0 days for sheep and cattle, respectively) for the 10 days after the introduction of movement restrictions. (**C**) The observed mean report-to-slaughter delay by day of report, demonstrating the improvements achieved in quickly slaughtering animals on infected holdings. GB, Great Britain. (**D**) Data and fitted distributions of the report-to-slaughter delay for cases reported between 1 and 10 March 2001. A long tail in the report-to-slaughter distribution is cause for concern because of the high potential for (avoidable) transmission during this interval. Distributions were fitted with gamma distributions representing multiple convoluted exponential distributions to allow representation within the compartmental dynamical model (*15*).

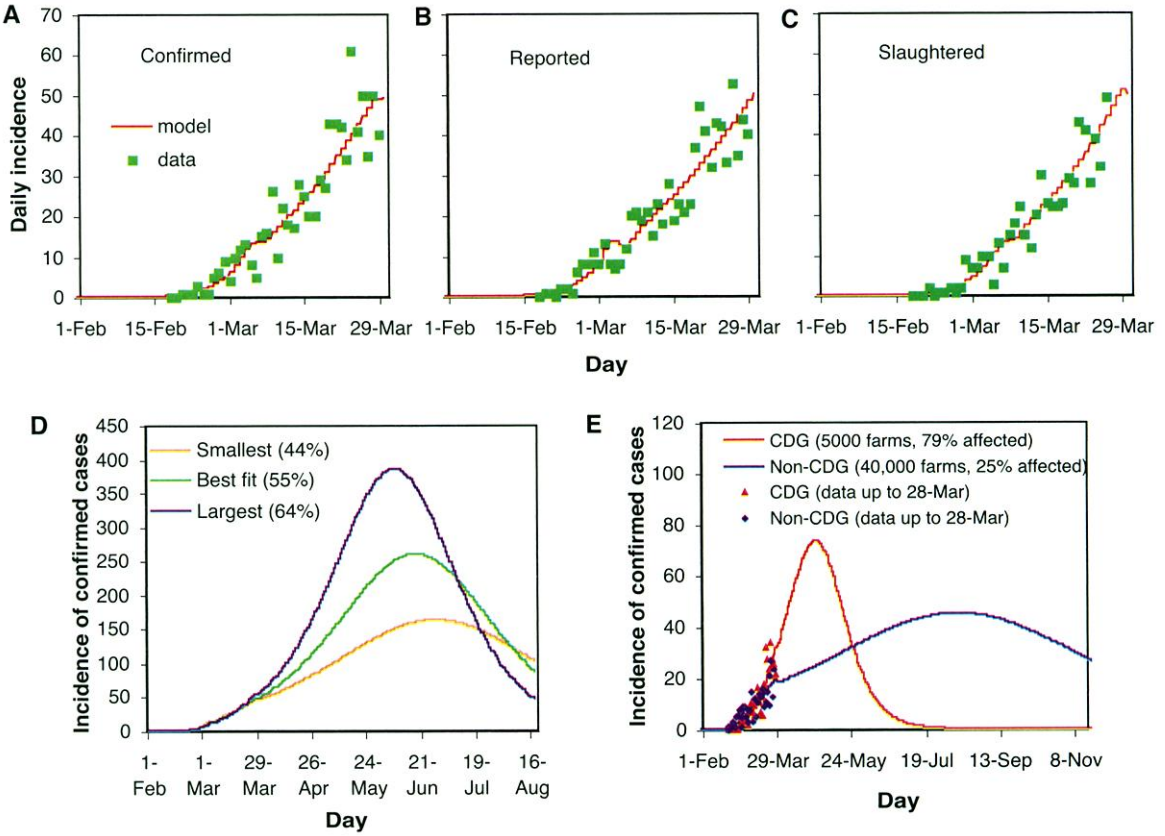

Fig. 3. Observed and fitted time series for (**A**) confirmed, (**B**) reported, and (**C**) slaughtered FMD cases are presented for the best fit model (estimated date of first infection T_0 = 5 February 2001, R_0 = 8.4 on 22 February 2001, R_0 = 1.7 on 24 February 2001, and R_0 = 1.3 on 28 March 2001, ϕ = 0.11). The data are overdispersed with an estimated variance to mean ratio of 1.5, reducing the quality of fit achieved to p = 0.02 and complicating identification of the time at which the epidemic peaks. Not allowing for parameter uncertainty, approximate prediction intervals on all curves are $\pm 2.4\sqrt{x}$, where x is the predicted value. (**D**) Predictions of confirmed case incidence are presented for this model along with those from the models with epidemic sizes at the upper and lower 95% confidence limits of R_0 estimated on 28 March 2001 (largest epidemic scenario: T_0 = 5 February 2001, R_0 = 7.8 on 22 February 2001, R_0 = 1.4 on 28 March 2001; smallest scenario: T_0 = 6 February 2001, R_0 = 9.8 on 22 February 2001, R_0 = 1.2 on 28 March 2001). Numbers in parentheses represent the proportion of farms infected. (**E**) Predicted epidemic sizes in the CDG infected area versus all other infected areas. For CDG, analysis of spatial distance data gives ϕ = 0.12, n = 5.5, and model fitting gives R_0 = 36 on 22 February 2001, R_0 = 1.6 on 28 March 2001, T_0 = 15 February 2001. For non-CDG regions, ϕ = 0.07, n = 8.3, and model fitting gives R_0 = 6.7 on 22 February 2001, R_0 = 1.1 on 28 March 2001, T_0 = 5 February 2001. Estimates of pre–movement ban R_0 are confounded with T_0 estimates. Predictions shown assume that the distributions of times from report to confirmation or slaughter of index cases remain unchanged after 28 March 2001. Results for r_I = 1 alone are shown here, because fit quality and resulting epidemic size varied little with the parameter.

to consider other interventions, particularly those capable of rapidly controlling infection that is established in multiple regions.

In this context, ring culling or vaccination strategies target infection hotspots by reducing the density of susceptible farms in the vicinity of diagnosed infections, thereby removing the "fuel" essential to maintaining the epidemic. More aggressive preemptive slaughter of animals potentially in contact has been adopted in other European countries with low case numbers to date (France, Ireland, and the Netherlands) and is now being implemented in Great Britain through the culling of farms contiguous to an index case. The current policy (*1*), based in part on these analyses, is to cull infected premises within 24 hours of report and neighboring (contiguous) farms within 48 hours. Encouraging progress has been made recently (Fig. 2C). Our analysis shows that both ring culling (Fig. 4B) (rapidly slaughtering all animals within a certain radius of every newly diagnosed case of infection) and ring vaccination (vaccinating rather than culling animals on the same time scale) are both potentially highly effective strategies if implemented sufficiently rigorously. The relationship between the benefits gained (in terms of both infections prevented and the total number of farms requiring culling) is highly nonlinear, however, because the maximum benefits are only gained by aggressive policies that reduce transmission below the critical level required for the epidemic to be self-sustaining. Clear communication of this basic epidemiological principle is key when justifying such a policy, as demonstrated by the delays in implementation of ring culling in Great Britain in March caused by protests by the farming community. Policies can be overaggressive, however: a 3-km ring cull is predicted to result in more farms being culled to eliminate the disease than a 1.5-km cull (Fig. 4B). This trade off is more acute if $r_I > 1$, where ring culling still accelerates the decline of the epidemic but at the cost of a larger cull than rapid index case slaughtering alone. This dilemma heightens the need for future research to quantify how farm infectiousness depends on time from initial FMD infection (*20*).

Ring vaccination policies need to be more extensive than comparable culling policies, because vaccination has little effect on the infectiousness of animals already infected with the virus. Hence, culling reduces the susceptible population and reduces transmission by removing infected (but undiagnosed) animals, whereas vaccination essentially only achieves the former (*17*). However, although Fig. 4C shows how ring vaccination can reduce the size of the epidemic, this impact is at the cost of needing to vaccinate a much larger number of animals than would be required to be culled under a ring culling policy achieving the same effect. Given that vaccinated animals need to be culled later in order for export restrictions to be lifted (no antibody-positive animals may be exported at present, regardless of the cause of acquisition of immunity), this finding further questions the cost-benefit ratio of such vaccination policies. However, additional cost-benefit analyses comparing vaccination with culling that take account of any differences in the costs of policy implementation are urgently required. The impact of control policies on different areas is broadly similar, despite apparent regional differences in R_0 (Fig. 3E), as shown in Fig. 4D where a variety of possible control

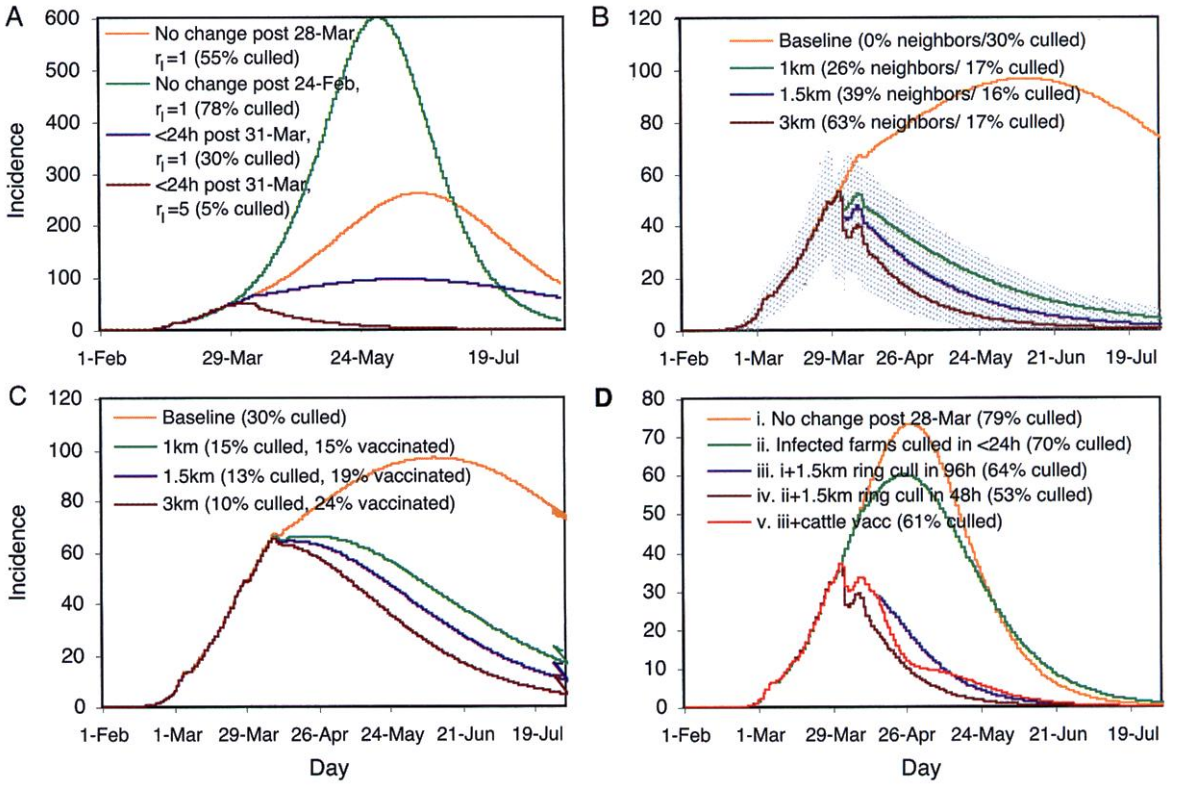

Fig. 4. (**A**) Predicted case incidence for baseline scenario (R_0 = 1.3) compared with scenario in which time-to-confirmation and time-to-slaughter distributions remained fixed after 24 February 2001 (R_0 = 1.7) and with two scenarios in which mean time to slaughter is reduced to 12 hours after 31 March 2001 (R_0 = 1.1 for r_I = 1, R_0 = 0.7 for r_I = 5). This shows the effect of improvements in control after the movement ban and the benefits of achieving the government objective of culling all suspect cases within 24 hours. Percentages in parentheses represent the proportion of farms culled or vaccinated during the entire epidemic. The scenario with r_I = 5 results in many fewer farms culled than do the r_I = 1 scenarios. (**B**) Predicted effect of ring culling and (**C**) ring vaccination of all animals at radius 1, 1.5, and 3 km from FMD-affected farms, introduced on 1 April 2001. The gray-shaded area in (B) represents the 95% prediction intervals around the 1.5-km ring cull scenario, allowing for uncertainty in R_0 estimates. The proportion of the contact neighborhood falling within a ring is listed in parentheses. Vaccination is optimistically assumed to be fully protective after 3 days for susceptible animals, with protection lasting for the duration of the current epidemic, but not to affect the infectivity of animals already infected. The baseline scenario in (B) and (C) assumes that culling of suspect cases within 24 hours is achieved by 1 April 2001. Otherwise, ring culling is less effective (for example, 26% of farms affected for a 1.5-km cull). (**D**) Intervention scenarios in the CDG region: (i) current (28 March 2001) slaughter time, no ring cull; (ii) slaughtering on all infected farms in <24 hours; (iii) scenario (i) plus 1.5-km ring cull performed in 96 hours; (iv) scenario (ii) plus 1.5-km ring cull in 48 hours; (v) scenario (iii) plus vaccination of all cattle carried out from 3 to 12 April 2001, assumed to protect 35% of farms (with cattle only) completely and reduce the infectivity of other farms by 17% (17% equals the fraction of animals that are cattle on mixed farms). Delays in introduction always reduce the effect of intervention. Scenarios shown in (B) through (D) assume r_I = 1; ring culling and vaccination also speed declines in case incidence for larger r_I but can involve more farms being culled than for an infected farm culling policy alone [for example, for the r_I = 5 scenario in (A), adding a 1.5-km ring cull policy increases the proportion of farms culled to 10%]. When comparing with case data, note that the projections in this figure do not include potential additional incidence reductions caused by ongoing voluntary and welfare-related culling schemes.

options for the infection hotspot of the CDG region are explored. This analysis also demonstrates how delays imposed by logistical limitations on culling rates may not substantially affect the impact of control policies but may result in larger cull numbers overall. Within the context of an effective rapid slaughter and ring cull policy, vaccination of cattle in the CDG region is also shown to have little impact in controlling the epidemic, though it does temporarily prevent the need to slaughter up to about 90,000 cattle on ring-culled farms.

Ever-increasing international trade has greatly increased the potential for the spread of FMD, as animals are more frequently moved over long distances. A thorough international review of policy options is required, focusing on the following issues: minimizing the potential for reintroduction of the virus from countries with endemic infection; the development of a robust serological test to discriminate between immunity induced by vaccination from that induced by infection; a cost-benefit analysis of mass vaccination options versus cull-based control of infrequent outbreaks; logistical improvements to minimize delays from report to slaughter; and optimizing preemptive culling strategies. However, extensive culling is sadly the only option for controlling the current British epidemic, and it is essential that the control measures now in place be maintained as case numbers decline to ensure eradication.

References and Notes

1. See the British Ministry of Agriculture, Fisheries and Food Web site at www.maff.gov.uk/.
2. J. Gloster, R. M. Blackall, R. F. Sellers, A. Donaldson, *Vet. Rec.* **108**, 370 (1981).
3. M. E. Hugh-Jones, P. B. Wright, *J. Hyg.* **68**, 253 (1970).
4. A. I. Donaldson, T. R. Doel, *Vet. Rec.* **131**, 114 (1992).
5. T. R. Doel, L. Williamson, P. V. Barnett, *Vaccine* **12**, 592 (1994).
6. S. J. Cox *et al.*, *Vaccine* **17**, 1858 (1999).
7. J. S. Salt *et al.*, *Vaccine* **16**, 746 (1998).
8. M. E. J. Woolhouse, A. Donaldson, *Nature* **410**, 515 (2001).
9. The probability density function, $f_i(r)$, of the distance, r, from the source FMD-affected farm to the farms it infects was parameterized as $f_i(r) = p\kappa(r)/N + (1 - p)g(r)$, with probability p that the infection arose uniformly over the area surrounding the index case (representing mass action mixing) and probability $(1 - p)$ that the infection arose from local spread in the proximity of the FMD-affected farm characterized by contact kernel $g(r)$. The total number of farms, N, and the radial density of farms with sheep, cattle, and/or pigs distance r from the average FMD-affected farm, $\kappa(r)$, were determined by data from the June 2000 Agricultural and Horticultural Census (*19*). Using the following parametric model of the kernel

$$g(r) = \exp(-\alpha r^{\beta})\kappa(r) \Big/ \int_0^{\infty} \exp(-\alpha r^{\beta})\kappa(r)dr$$

we obtained parameter estimates (α = 3.5, β = 0.39, and p = 0.21 and 0.04, before and after movement restrictions, respectively) by fitting $f_i(r)$ to the distribution of distances r between identified infectious contacts.
10. R. M. Anderson, R. M. May, *Infectious Diseases of Humans* (Oxford Univ. Press, 1991).
11. R_0 was estimated from contact data by multiplying the average number of infectious days by the average number of farms infected per infectious day, correcting for the proportion of farms for which no source of infection was identified. We assumed constant infec-

tiousness from 3 days after infection until slaughter (for an average of eight infectious days).

12. The effective neighborhood size, n, in units of nearest neighbor farms, was estimated as

$$n = \int_0^\infty g(r)dr \Big/ \int_0^R g(r)dr$$

where R is given by the solution of

$$\int_0^R \kappa(r)dr = 1$$

The connectedness of the contact network is given by

$$\phi = \frac{1}{n^2} \int\int\int g(r)g(r')g(|\mathrm{r} - \mathrm{r}'|)/\kappa(|\mathrm{r} - \mathrm{r}'|)drdr'd\theta$$

where

$$|\mathrm{r} - \mathrm{r}'| = r^2 + r'^2 - 2rr'\cos(\theta)$$

13. S. C. Howard, C. A. Donnelly, *Res. Vet. Sci.* **69**, 189 (2000).
14. D. T. Haydon, M. E. J. Woolhouse, R. P. Kitching, *IMA J. Math. Appl. Med. Bio.* **14**, 1 (1997).
15. The population of farms was stratified into a susceptible class, S; sequential infection classes, I_i ($i = 1..M$); and a slaughtered/vaccinated class, D. Multiple infected classes were used to exactly reproduce the gamma distribution fits to the delay data shown in Fig. 2 and to represent different stages of infectiousness and diagnosis. The mixture model of the infection-to-report distribution was represented by overlapping sets of 30 classes (transit time = 0.26 days each, weight 0.82) and 4 classes (transit times = 3.73 days, weight 0.18). Two classes (transit times = 0.85 to 0.21 days, time-dependent) represented farms awaiting disease confirmation after report, and four classes (transit times = 0.82 to 0.38 days, time-dependent)—overlapping the previous two—represented farms awaiting culling after disease reporting. Infectiousness varies as a function of incubation stage, reaching significant levels after around 3.5 days and then continuing at a constant level until diagnosis, after which it remains constant until slaughter at a level r_I times greater than before reporting. The model is novel in tracking not only the numbers of farms in each infection state through time, but also the numbers of pairs of farms connected on the contact network used to represent spatially localized disease transmission. For conciseness and clarity, we only present those for a simpler model with only two infected classes: E (uninfectious) and I (infectious). Using $[X]$ to represent the mean number in state X, $[XY]$ to represent the mean number of pairs of type XY, and $[XYZ]$ to represent the mean number of triples, the dynamics can be represented by the following set of differential equations: $d[S]/dt = -(\tau + \mu + \omega)[SI] - p\beta[S][I]/N$, $d[E]/dt = p\beta[S][I]/N + \tau[SI] - \nu[E] - \mu[EI]$, $d[I]/dt = \nu[E] - s[I] - \mu[II]$, $d[SS]/dt = -2(\tau + \mu + \omega)[SSI] - 2p\beta[SS][I]/N$, $d[SE]/dt = \tau([SSI] - [ISE]) - \mu([SEI] + [ISE]) - \omega[ISE] + p\beta([SS] - [SE])[I]/N$, $d[SI]/dt = \nu[SE] - (\tau + \mu + \omega)([ISI] + [SI]) - p\beta[SI][I]/N$, $d[EE]/dt = \tau[ISE] - 2\mu[EEI] - 2\nu[EE] + 2p\beta[SE][I]/N$, $d[EI]/dt = \nu[EE] - \mu([EI]+[IEI]) - (\nu + \sigma)[EI] + p\beta[SI][I]/N$, $d[II]/dt = 2\nu[EI] - 2\sigma[II] - 2\mu([II] + [III])$. The numbers of triples are calculated with the closure approximation (*16*) $[XYZ] \approx (n - 1)[XY][YZ](1 - \phi + \phi\, N[YY]/n[X][Z])/n[Y]$, where n is the mean contact neighborhood size of a farm, ϕ is the proportion of triples in the network that are triangles, and N is the total number of farms [see (*12*)]. $\tau = (1 - p)\beta/n$ is the transmission rate across a contact, where β is the transmission coefficient of the virus, and p is the proportion of contacts that are long-range [see (*9*)], both of which are estimated separately before and after the movement ban. ν is the rate of transit from the uninfectious to the infectious class, and σ is the rate of transit from the infectious to the removed class. μ is the rate at which farms in the neighborhood of an infected farm are culled in ring culling, and ω is the rate at which farms are vaccinated in ring vaccination. It is assumed that vaccination has no effect on previously infected farms.
16. M. J. Keeling, *Proc. R. Soc. London B* **266**, 859 (1999).
17. Removal by culling of an infected herd and the removal of contiguous holdings of animals have different impacts on R_0 and the scale of the epidemic. The former acts directly to reduce R_0, whereas the latter serves to significantly reduce the overall scale of the epidemic by stopping second-generation transmission events [hence reducing the effective reproductive number (*10*)].
18. *Northumberland Report: The Report of the Committee of Inquiry on Food and Mouth Disease* (Her Majesty's Stationery Office, London, 1968).
19. June 2000 Agricultural and Horticultural Census, Ministry of Agriculture, Fisheries and Food, National Assembly for Wales Agriculture Department and Scottish Executive Rural Affairs Department; Crown copyright, 2001.
20. The rapid decline in case incidence seen after completion of the analysis presented in this paper has given new estimates of r_I significantly above 1, though more precise estimation awaits availability of detailed data on all slaughter schemes in operation since 30 March 2001.

21. We are extremely grateful for help in the provision of data and for invaluable advice from J. Wilesmith (Veterinary Laboratory Agency), D. Reynolds (Food Standards Agency and Ministry of Agriculture, Fisheries and Food), and D. Thompson (Ministry of Agriculture, Fisheries and Food) and to the many government epidemiologists and veterinary staff who collected the unique contact tracing data on FMD spread in the current epidemic. In addition, we thank D. King (Office of Science and Technology), B. Grenfell, M. Keeling, M. Woolhouse, and other members of the FMD Official Science Group for stimulating discussions; Sir Robert May and Sir David Cox for valuable advice and discussions; three anonymous referees for comments; and S. Dunstan, S. Riley, and H. Carabin for valuable assistance. N.M.F. thanks the Royal Society and the Howard Hughes Medical Institute for fellowship and research funding support. C.A.D. and R.M.A. thank the Wellcome Trust for research funding.

23 March 2001; accepted 10 April 2001
Published online 12 April 2001;
10.1126/science.1061020
Include this information when citing this paper.

Structural Mechanism for Statin Inhibition of HMG-CoA Reductase

Eva S. Istvan[1] and Johann Deisenhofer[1,2]*

HMG-CoA (3-hydroxy-3-methylglutaryl–coenzyme A) reductase (HMGR) catalyzes the committed step in cholesterol biosynthesis. Statins are HMGR inhibitors with inhibition constant values in the nanomolar range that effectively lower serum cholesterol levels and are widely prescribed in the treatment of hypercholesterolemia. We have determined structures of the catalytic portion of human HMGR complexed with six different statins. The statins occupy a portion of the binding site of HMG-CoA, thus blocking access of this substrate to the active site. Near the carboxyl terminus of HMGR, several catalytically relevant residues are disordered in the enzyme-statin complexes. If these residues were not flexible, they would sterically hinder statin binding.

Elevated cholesterol levels are a primary risk factor for coronary artery disease. This disease is a major problem in developed countries and currently affects 13 to 14 million adults in the United States alone. Dietary changes and drug therapy reduce serum cholesterol levels and dramatically decrease the risk of stroke and overall mortality (*1*). Inhibitors of HMGR, commonly referred to as statins, are effective and safe drugs that are widely prescribed in cholesterol-lowering therapy. In addition to lowering cholesterol, statins appear to have a number of additional effects, such as the nitric oxide–mediated promotion of new blood vessel growth (*2*), stimulation of bone formation (*3*), protection against oxidative modification of low-density lipoprotein, as well as anti-inflammatory effects and a reduction in C-reactive protein levels (*4*). All statins curtail cholesterol biosynthesis by inhibiting the committed step in the biosynthesis of isoprenoids and sterols (*5*). This step is the four-electron reductive deacylation of HMG-CoA to CoA and mevalonate. It is catalyzed by HMGR in a reaction that proceeds as follows

$$\text{(S)-HMG-CoA} + 2\text{NADPH} + 2\text{H}^+ \rightarrow \text{(R)-mevalonate} + 2\text{NADP}^+ + \text{CoASH}$$

where $NADP^+$ is the oxidized form of nicotinamide adenine dinucelotide, NADPH is the reduced form of $NADP^+$, and CoASH is the reduced form of CoA.

Several statins are available or in late-stage clinical development (Fig. 1). All share an HMG-like moiety, which may be present in an inactive lactone form. In vivo, these prodrugs are enzymatically hydrolyzed to their active hydroxy-acid forms (*5*). The statins

[1]Department of Biochemistry, [2]Howard Hughes Medical Institute, University of Texas Southwestern Medical Center at Dallas, TX 75390–9050, USA.

*To whom correspondence should be addressed. E-mail: Johann.Deisenhofer@UTSouthwestern.edu